

The Nelder–Mead Method-Based Improved Parameter Estimation of Single-Phase Induction Motors

Research paper

Son T. Nguyen^{1,*}, Tu M. Pham¹, Anh Hoang¹, Linh V. Trieu¹, Trung T. Cao¹, Tuan V. Pham²

¹Department of Electrical Engineering, School of Electrical and Electronic Engineering, Hanoi University of Science and Technology, Hanoi, Vietnam

²Department of Electrical and Electronic Technology, Faculty of Electrical and Electronics, Vinh University of Technology Education, Vinh, Vietnam

Received: 03 June 2024; Accepted: 23 September 2024

Abstract: This work presents a comprehensive method for precisely determining the equivalent circuit characteristics of single-phase induction motors (SPIM), including both direct and indirect steps. First, a DC test, a no-load test and a locked-rotor test are performed to ascertain the primary electrical characteristics of both the main and auxiliary windings. Next, the indirect phase consists of iteratively modifying the mechanical characteristics, such as the inertial moment and friction factor, in a motor simulation model in Simulink until they match the previously determined electrical parameters. In addition, the motor parameter estimate process can be improved by applying the Nelder–Mead optimisation approach, which eliminates the need to calculate partial derivatives of a cost function. The study also applies the scalar control to the SPIM. Ultimately, the efficacy of the suggested methodology is confirmed through a comparison of simulated and actual outcomes.

Keywords: single-phase induction motor • parameter estimation • the Nelder–Mead optimisation method • scalar control

1. Introduction

The single-phase induction motor (SPIM) is frequently used in various household appliances, including fans, water pumps and air blowers (Nied, 2013; Rahman et al., 2020; Saneie and Nasiri-Gheidari, 2021; Sharma and Singh, 2021; Wang et al., 2010). The SPIM is also utilised for small-scale industrial machinery in situations where there is a lack of three-phase power sources. SPIMs can be classified into split-phase motors, capacitor-run or capacitor-start motors, and shaded-pole motors (Jang, 2013).

Unlike three-phase induction motors, the design approach for the SPIM focuses on the limitation of not being able to generate circular rotating fields. To accomplish this, the main winding of the motor is specifically engineered to produce a circular rotating magnetic field and limit the loss of electrical energy through the copper components (Um and Park, 2019). In addition, an ideal SPIM design entails the examination of various rotor slot configurations (Kim et al., 2009). An aggregate SPIM model is necessary to analyse the overall system performance when numerous SPIMs are employed simultaneously to enhance power to the load (Poudel et al., 2019).

Until now, the permanent split capacitor (PSC) motor, which is a type of split-phase motor, has been widely used in various industrial and residential applications. The PSC motor is typically constructed with two windings: main and auxiliary. The main winding is directly connected to the power supply. Meanwhile, the auxiliary winding is indirectly connected to the power supply via a capacitor. When the motor operates with a single-phase power supply, the role of the capacitor is generating a waveform close to a two-phase power supply and generating a rotating magnetic field.

* Email: son.nguyenthanh@hust.edu.vn

The characteristics of the motor equivalent circuit are often determined by conducting a sequence of tests, including a DC test, a no-load test and a locked-rotor test. These tests consider the effective turn ratio of the auxiliary and main windings. If this ratio is not accessible, it can be replaced by using a calculated complex voltage ratio (Ghial et al., 2014). The categorisation of parameter estimate for single-phase motors can be divided into two groups: offline approaches (Huynh et al., 2015; Ojaghi and Daliri, 2016) and online methods (Vieira et al., 2009). Online estimation methods usually need the utilisation of power converters and additional controllers, with the inclusion of the motor parameter estimation method in the entire control algorithm. By contrast, offline estimating approaches use fewer devices or eliminate the requirement for extra controllers. However, conventional offline estimating methods have not considered the influence of temperature changes on motor parameters.

Analysing the behaviour and performance of an SPIM typically requires studying the motor's equivalent circuit. This information is crucial for assessing the state and performance of the motor (Bhowmick et al., 2018). The motor's parameters are also essential for motor vector control systems (Correa et al., 2004). Moreover, in several applications of SPIM drives, accurately determining the motor parameters is crucial for the development of speed sensorless control algorithms (Jannati and Fallah, 2011; Vendrusculo and Pomilio, 2008).

Current studies have mostly concentrated on variable-speed drives for SPIMs, resulting in notable advancements (Almani et al., 2021; Jemli et al., 2009). The speed control methods for SPIMs, like three-phase induction motors, can be categorised into scalar control methods (Dangeam and Kinnares, 2015; Jidin et al., 2005; Schraud et al., 2008; Sutedjo et al., 2018) and vector control methods (Aller et al., 2018; Correa et al., 2004; Jang, 2013; Nied, 2013; Rubio-Astorga et al., 2014). Efficiency optimisation control for SPIMs can be achieved by a motor efficiency analysis, as demonstrated by Zahedi and Vaez-Zadeh (2009), and Asadabadi (2011). These experiments focused on designing controllers that could regulate motor speed without causing any significant increase in motor loss when operating under non-rated conditions.

This study presents a two-step approach for calculating the equivalent circuit characteristics of a small-scale PSC induction motor. Initially, temporary parameters are acquired through a DC test, no-load test and locked-rotor test for both the primary and secondary windings. Subsequently, these provisional parameters are employed as an initial condition for the Nelder–Mead method-based optimisation process to improve the precision of estimating circuit parameters of the primary and auxiliary windings. The benefit of using the Nelder–Mead optimisation method is that it does not require any derivative of the objective function. Indeed, the Nelder–Mead optimisation method is very suitable for this study as the derivatives of objective functions are impossible to be computed. However, the Nelder–Mead method is a heuristic search method that can converge to non-stationary points on problems that can be initiated by other methods. This problem can be overcome if an appropriate initial condition can be given before the Nelder–Mead optimisation process starts. Finally, this study also presents a basic motor control system by utilising the scalar control algorithm with the exploration of an (STMicroelectronics company) STM32F4 microcontroller.

2. Parameter Estimation of SPIMs Using Measurement Tests

Figures 1 and 2 depict the corresponding circuits for the main and auxiliary windings of the widely used SPIM, respectively (Huynh et al., 2015). Like three-phase induction motors, the SPIM can also be built with a squirrel-cage rotor. Table 1 provides the specifications of the main and auxiliary windings of the SPIM. The main winding is connected to a single-phase voltage source V_s , while the slip rate s represents the difference between the synchronous speed and the actual speed of the motor.

2.1. Main winding parameter estimation

The parameters of the main winding's equivalent circuit can be approximated by conducting the following experiments:

- DC test
- No-load test
- Locked rotor test

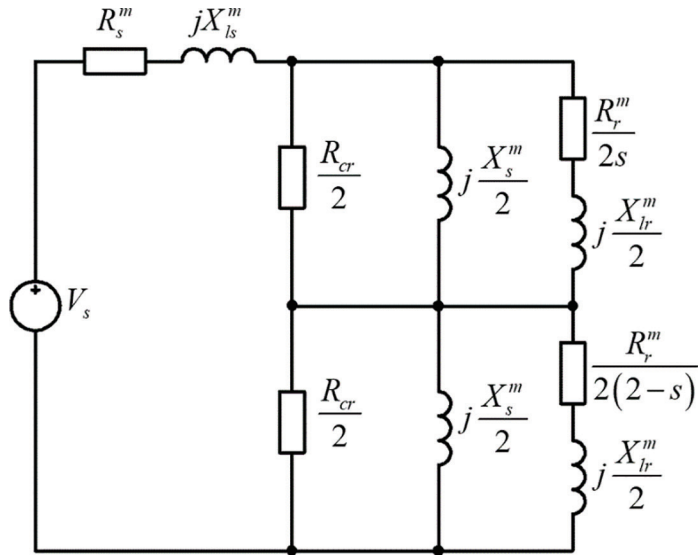


Figure 1. Equivalent circuit of the main winding.

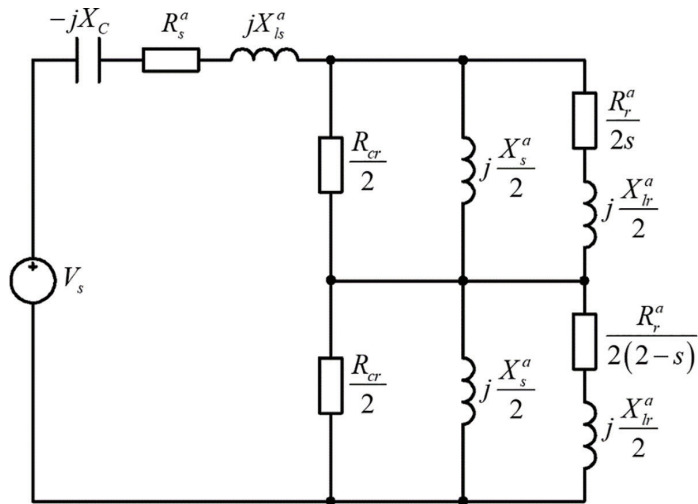


Figure 2. Equivalent circuit of the auxiliary winding.

Table 1. List of SPIM parameters.

R_s^m	Resistance of the main winding
X_{ls}^m	Leakage reactance of the stator of the main winding
X_s^m	Self-reactance of the main winding
X_{lr}^m	Leakage inductance of the rotor referred to the stator side of the main winding
R_r^m	Resistance of the rotor referred to the stator side of the main winding
R_s^a	Resistance of the auxiliary winding
X_{ls}^a	Leakage reactance of the auxiliary winding
X_s^a	Self-reactance of the auxiliary winding
X_{lr}^a	Leakage inductance of the rotor referred to the stator side of the auxiliary winding
R_r^a	Resistance of the rotor referred to the stator side of the auxiliary winding
R_{cr}	Core-loss resistance

SPIM, single-phase induction motor.

2.1.1. DC test

This step can be easily accomplished by using a low DC voltage applied to the main winding and the current in the winding is measured. The DC resistance of the main winding R_s^m is equal to the supplied voltage divided by the measured current.

2.1.2. No-load test

During this experiment, the rotor was rotated at a speed that was very close to a nearly synchronous speed, and the slip was a very small value. The values of the terminal voltage V_{NL}^m , current I_{NL}^m , active power P_{NL}^m and reactive power Q_{NL}^m need to be calculated with the following assumptions taken into account:

- The core-loss resistance, R_{cr} , is large enough to be abolished;
- Due to a small slip rate s , the term $R_r^m/2s$ is very large to be ignored;
- In most SPIMs, the self-reactance X_s^m is usually much larger than the rotor leakage reactance referred to the stator side X_{lr}^m ($X_s^m \gg X_{lr}^m$);
- The self-reactance X_s^m is also much larger than the rotor resistance referred to the stator side R_r^m ($X_s^m \gg R_r^m$).

Figure 3 displays the circuit that represents the main winding in the no-load test. The total reactance of the circuit is determined as follows:

$$X_{NL}^m = \frac{\sqrt{(V_{NL}^m I_{NL}^m)^2 - (P_{NL}^m)^2}}{(I_{NL}^m)^2} \quad (1)$$

where

- V_{NL}^m : Voltage applied to the main winding;
- I_{NL}^m : Current in the main winding;
- P_{NL}^m : Actual power of the main winding.

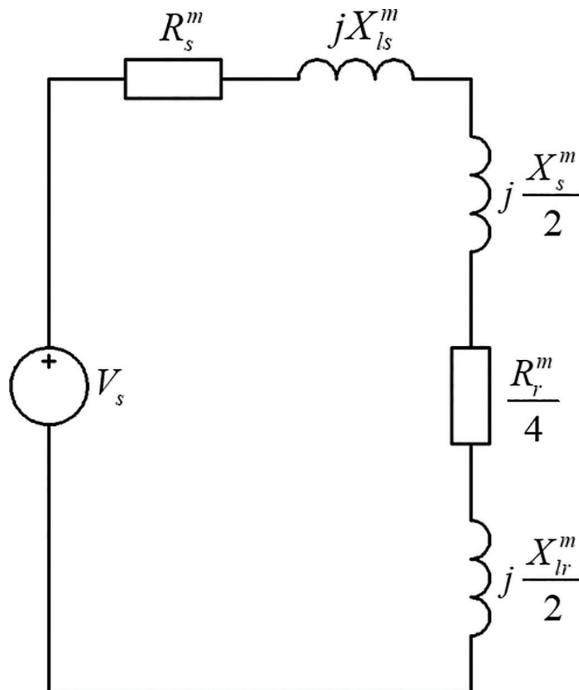


Figure 3. Equivalent circuit of the main winding under the no-load test.

The values of V_{NL}^m , I_{NL}^m and P_{NL}^m in Eq. (1) can be directly determined through measurement. Based on the circuit depicted in Figure 3, the calculation for X_{NL}^m is as follows:

$$X_{NL}^m = X_{ls}^m + 0.5X_s^m + 0.5X_{lr}^m \quad (2)$$

By employing Eq. (2), the value of X_s^m can be determined in the following manner:

$$X_s^m = 2(X_{NL}^m - X_{ls}^m - 0.5X_{lr}^m) \quad (3)$$

2.1.3. Locked rotor test

When the rotor is locked from rotating, the slip rate $s = (n_1 - n)/n_1 = 1$. Additionally, the following assumptions are made:

- The self-reactance X_s^m is significantly higher than the leakage inductance of the rotor referred to the stator side X_{lr}^m ($X_s^m \gg X_{lr}^m$);
- The self-reactance X_s^m is significantly higher than the resistance of the rotor referred to the stator side R_r^m ($X_s^m \gg R_r^m$).

Thus, the circuit representing the main winding during the lock-rotor test is as shown in Figure 4.

Using Figure 4 the aggregate resistance is given as follows:

$$R_{LR}^m = \frac{P_{LR}^m}{(I_{LR}^m)^2} = R_s^m + R_r^m \quad (4)$$

Using Eq. (4), the resistance of the rotor referred to the stator side R_r^m is computed as follows:

$$R_r^m = R_{LR}^m - R_s^m \quad (5)$$

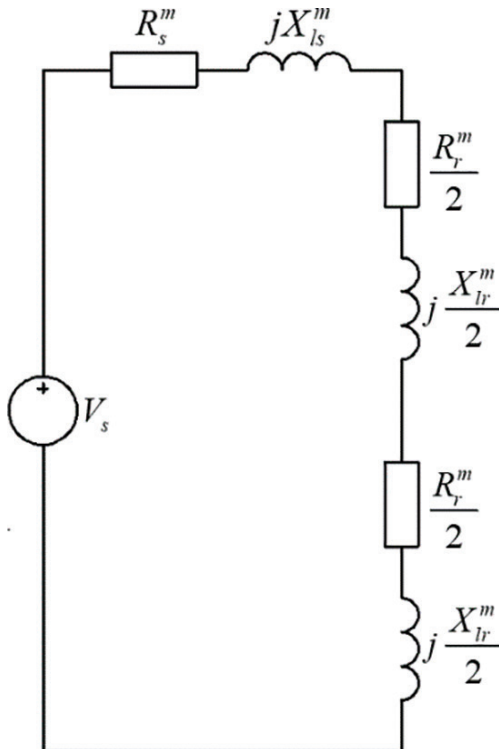


Figure 4. Equivalent circuit of the main winding under the locked-rotor test.

The aggregate reactance is also given as follows:

$$X_{LR}^m = \frac{\sqrt{\left(V_{LR}^m I_{LR}^m\right)^2 - \left(P_{LR}^m\right)^2}}{\left(I_{LR}^m\right)^2} \quad (6)$$

where

- V_{LR}^m is the root mean square (RMS) value of the voltage applied to the main winding during the locked rotor test;
- I_{LR}^m represents the RMS value of the current flowing through the main winding during the locked rotor test;
- P_{LR}^m represents the real power of the main winding during the locked rotor test.

According to Eq. (6), V_{LR}^m , I_{LR}^m and P_{LR}^m are directly measured in the locked-rotor test. The stator leakage reactance X_{ls}^m and the rotor leakage reactance referred to the main winding X_{lr}^m are usually considered to be equal and they can be calculated as follows.

In the locked-rotor test, V_{LR}^m , I_{LR}^m and P_{LR}^m are directly measured. The stator leakage reactance, X_{ls}^m , and the rotor leakage reactance referred to the stator side, X_{lr}^m , are typically assumed to be equivalent. These values can be computed using the following formulas:

$$X_{ls}^m = X_{lr}^m = \frac{X_{LR}^m}{2} \quad (7)$$

Substituting Eq. (7) into Eq. (3) gives:

$$X_s^m = 2 \left(X_{NL}^m - \frac{3}{4} X_{LR}^m \right) \quad (8)$$

The process of determining the parameters of the main winding involves the following steps:

- Step 1: Measuring the DC resistance of the main winding R_s^m using a DC test;
- Step 2: Calculating the leakage reactance of the stator X_{ls}^m and the leakage inductance of the rotor referred to the stator side X_{lr}^m using Eq. (7);
- Step 3: Calculating the self-reactance X_s^m using Eq. (8);
- Step 4: Calculating the resistance of the rotor referred to the stator side R_r^m using Eq. (5).

2.2. Auxiliary winding parameter estimation

The parameters of auxiliary winding, like the main winding, are determined using the following tests:

- Direct current (DC) test;
- No-load test;
- Locked rotor test.

2.2.1. DC test

This step can be done by using a low DC voltage applied to the auxiliary winding and the current in the winding is measured. The DC resistance of the auxiliary winding R_s^a is equal to the supplied voltage divided by the measured current.

2.2.2. No-load test

In this test, the slip rate is negligible, hence the term $R_r^a / 2s$ can be considered significant and removed. Additionally, the following assumptions are made:

- The self-reactance X_s^a is much larger than the leakage reactance of the rotor referred to the stator side X_{lr}^a ($X_s^a \geq X_{lr}^a$);

- The self-reactance X_s^a is also much larger than the resistance of the rotor referred to the stator side R_r^a ($X_s^a \gg R_r^a$).

Thus, the circuit that represents the auxiliary winding in the no-load test can be observed in Figure 5. The total reactance of the circuit is determined as follows:

$$X_{NL}^a = \frac{\sqrt{(V_{NL}^a I_{NL}^a)^2 - (P_{NL}^a)^2}}{(I_{NL}^a)^2} \tag{9}$$

Based on the equivalent circuit of the auxiliary winding shown in Figure 5, the value of X_{NL}^a can be determined using the following calculation:

$$X_{NL}^a = -X_C + X_{ls}^a + \frac{1}{2}X_s^a + \frac{1}{2}X_{lr}^a \tag{10}$$

2.2.3. Locked rotor test

When the rotor is locked from rotating, the slip rate is $s = 1$. The subsequent assertions are presumed:

- The self-reactance X_s^a is significantly higher than the leakage inductance of the rotor referred to the stator side X_{lr}^a ($X_s^a \gg X_{lr}^a$);
- The self-reactance X_s^a is significantly higher than the resistance of the rotor referenced to the stator side R_r^a ($X_s^a \gg R_r^a$).

Thus, the circuit that represents the auxiliary winding during the locked rotor test is as depicted in Figure 6.

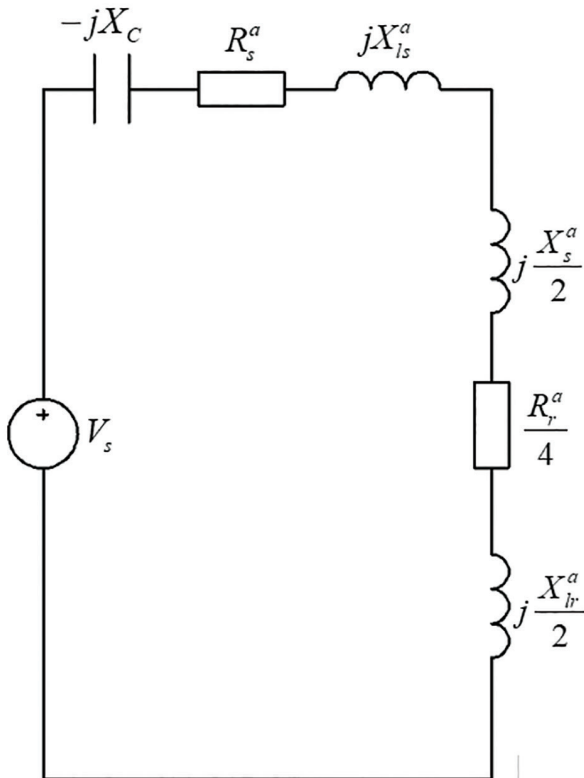


Figure 5. Equivalent circuit of the auxiliary winding under the no-load test.

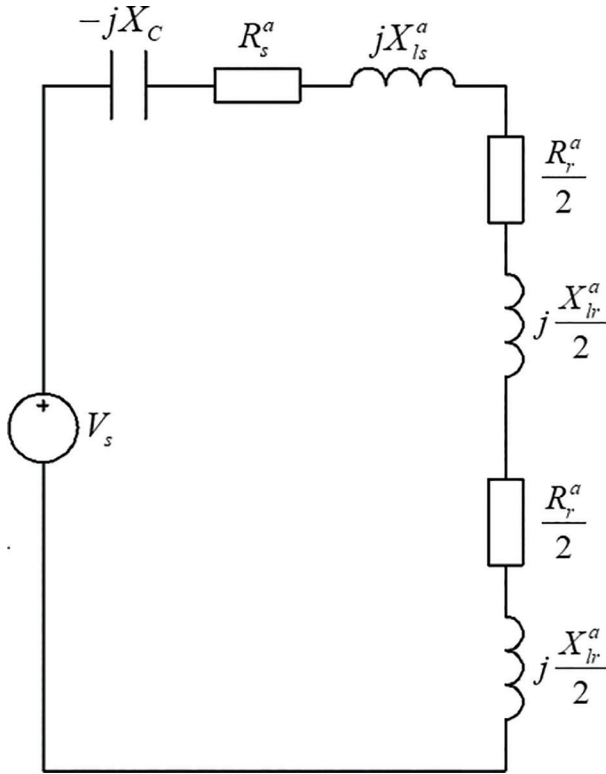


Figure 6. Equivalent circuit of the auxiliary winding under the locked-rotor test.

The aggregate reactance of the circuit can be determined using the following formula:

$$X_{LR}^a = \frac{\sqrt{(V_{LR}^a I_{LR}^a)^2 - (P_{LR}^a)^2}}{(I_{LR}^a)^2} \quad (11)$$

The stator leakage reactance X_{ls}^a and the rotor leakage reactance X_{lr}^a are typically assumed to be equivalent, hence they can be computed using the following formulas:

$$X_{ls}^a = X_{lr}^a = \frac{X_{LR}^a}{2} \quad (12)$$

Substituting Eq. (12) into Eq. (10) gives:

$$X_s^a = 2 \left(X_{NL}^a + X_C - \frac{3}{4} X_{LR}^a \right) \quad (13)$$

The total resistance of the circuit is determined as follows:

$$R_{LR}^a = \frac{P_{LR}^a}{(I_{LR}^a)^2} = R_s^a + R_r^a \quad (14)$$

The resistance of the rotor referred to the stator side can be determined using the following formula:

$$R_r^a = R_{LR}^a - R_s^a \quad (15)$$

The process of determining the parameters of the auxiliary winding involves the following steps:

- Step 1: Measuring the DC resistance of the auxiliary winding using a DC test;
- Step 2: Calculating the stator leakage reactance X_{ls}^a and the rotor leakage reactance using Eq. (12);
- Step 3: Calculating the self-reactance X_s^a using Eq. (13);
- Step 4: Calculating the resistance of the rotor R_r^a using Eq. (15).

3. Improved Parameter Estimation of SPIMs Using the Nelder–Mead Method

3.1. The Nelder–Mead method

Gradient descent techniques can be used to find the minimum or maximum of an objective function in a multidimensional space in optimisation problems. This requires evaluating the partial derivatives of the objective function. Nevertheless, in numerous instances, due to the challenging nature of obtaining partial derivatives of the target function, the Nelder–Mead technique might be regarded as an optimal alternative option (Lagarias et al., 1998). Nevertheless, the Nelder–Mead approach is a heuristic search algorithm that may converge to non-stationary locations for problems that can be addressed using alternative optimisation strategies. Therefore, selecting suitable initial values for variables is essential for this strategy to attain the needed convergence.

The Nelder–Mead method operates by generating a simplex of points throughout each iteration:

- Reflex
- Expand
- Contract outside
- Contract inside
- Shrink

To implement the Nelder–Mead approach, follow these steps:

Step 1: A simplex consists of points $x(i)$, $i = 1, \dots, n + 1$.

Step 2: The points in the simplex are arranged in ascending order based on their function values, from $f(x(1))$ (the lowest) to $f(x(n+1))$ (the highest). At each iteration, the current worst point $x(n+1)$ is removed and replaced with another point in the simplex.

Step 3: Calculate the point of reflection:

$$r = 2m - x(n+1) \tag{16}$$

where $m = \sum_{i=1}^n \frac{x_i}{n}$ and calculate $f(r)$.

Step 4: If $f(x(1)) \leq f(r) < f(x(n))$, the r is accepted and this iteration is ended (*Reflect*).

Step 5: If $f(r) < f(x(1))$, then generate the expand point s as follows:

$$s = m + 2(m - x(n+1)) \tag{17}$$

and calculate $f(s)$.

(a) If $f(s) < f(r)$, then s is accepted and the iteration is ended (*Expand*).

(b) Otherwise, r is accepted and the iteration is stopped (*Reflect*).

Step 6: If $f(r) \geq f(x(n))$, then a contraction is performed between m and the better of $x(n+1)$ and r .

(a) If $f(r) < f(x(n+1))$ (r is better than $x(n+1)$), then c is calculated as follows:

$$c = m + (r - m) / 2 \tag{18}$$

and calculate $f(c)$.

If $f(c) < f(r)$, then c is accepted and the iteration is ended (*Contract outside*).

Otherwise, Step 7 is continued (*Shrink*).

(b) If $f(r) \geq f(x(n+1))$, then generate cc as follows:

$$cc = m + (x(n+1) - m) / 2 \tag{19}$$

and calculate $f(cc)$.

If $f(cc) < f(x(n+1))$, then cc is accepted and the iteration is stopped (*Contract inside*).

Otherwise, Step 7 is continued (*Shrink*).

Step 7: The point n is computed as follows:

$$v(i) = x(1) + (x(i) - x(1)) / 2 \tag{20}$$

Compute $f(v(i))$, $i = 1, \dots, n+1$. At the next iteration, the simplex consists of $x(1), v(2), \dots, v(n+1)$ (*Shrink*).

Figure 7 shows points in the Nelder–Mead algorithm for calculations in the procedure.

3.2. Improved parameter estimation of SPIMs

The parameters of the main winding’s equivalent circuit ($R_s^m, X_{ls}^m, X_s^m, X_{lr}^m, R_r^m$) can be determined using the measurement procedures described in Section 2. These estimated parameters can then serve as the initial condition for an optimisation process aimed at improving the estimation of the motor’s parameters. In the optimisation problem used for parameter estimation in an SPIM, an objective function is defined as follows:

$$S_m = |R_{in}^m - R_m| + |X_{in}^m - X_m| = f(R_s^m, X_{ls}^m, X_s^m, X_{lr}^m, R_r^m) \tag{21}$$

R_m and X_m represent the measured input resistance and reactance, respectively, of the equivalent circuit of the main winding. R_{in}^m and X_{in}^m represent the input resistance and reactance of the equivalent circuit of the main winding, which are determined by the main winding characteristics ($R_s^m, X_{ls}^m, X_s^m, X_{lr}^m$ and R_r^m).

The calculations for R_{in}^m and X_{in}^m are as follows:

$$Z_1^m = R_s^m + jX_{ls}^m \tag{22}$$

$$Z_2^m = \left(\frac{1}{j \frac{X_s^m}{2}} + \frac{1}{\frac{R_r^m}{2s} + j \frac{X_{lr}^m}{2}} \right)^{-1} \tag{23}$$

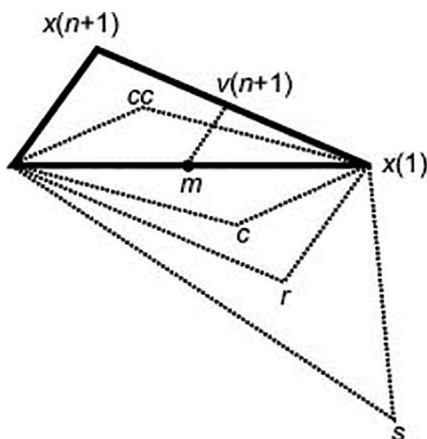


Figure 7. The principle of generating points in a simplex.

$$Z_3^m = \left(\frac{1}{j \frac{X_s^m}{2}} + \frac{1}{\frac{R_r^m}{2(2-s)} + j \frac{X_{lr}^m}{2}} \right)^{-1} \quad (24)$$

$$Z_{in}^m = Z_1^m + Z_2^m + Z_3^m \quad (25)$$

$$R_{in}^m = \text{real}(Z_{in}^m) \quad (26)$$

$$X_{in}^m = \text{imag}(Z_{in}^m) \quad (27)$$

The parameters of the auxiliary winding ($R_s^a, X_{ls}^a, X_s^a, X_{lr}^a, R_r^a$) can also be estimated using the same procedure for the main winding. An objective function is first defined as follows:

$$S_a = |R_{in}^a - R_a| + |X_{in}^a - X_a| = f(R_s^a, X_{ls}^a, X_s^a, X_{lr}^a, R_r^a) \quad (28)$$

where R_{in}^a and X_{in}^a represent the input resistance and reactance of the equivalent circuit of the auxiliary winding, which are determined by the auxiliary winding characteristics ($R_s^a, X_{ls}^a, X_s^a, X_{lr}^a$ and R_r^a).

R_{in}^a and X_{in}^a are as follows:

$$Z_1^a = R_s^a + jX_{ls}^a - jX_c^a \quad (29)$$

$$Z_2^a = \left(\frac{1}{j \frac{X_s^a}{2}} + \frac{1}{\frac{R_r^a}{2s} + j \frac{X_{lr}^a}{2}} \right)^{-1} \quad (30)$$

$$Z_3^a = \left(\frac{1}{j \frac{X_s^a}{2}} + \frac{1}{\frac{R_r^a}{2(2-s)} + j \frac{X_{lr}^a}{2}} \right)^{-1} \quad (31)$$

$$Z_{in}^a = Z_1^a + Z_2^a + Z_3^a \quad (32)$$

$$R_{in}^a = \text{real}(Z_{in}^a) \quad (33)$$

$$X_{in}^a = \text{imag}(Z_{in}^a) \quad (34)$$

4. Simulation and Experimental Results

Both experiment and simulation are necessary for the motor parameter estimate procedure. Figure 8 depicts an experimental apparatus comprising the subsequent components:

- A source of 220 VAC voltage;
- An SPIM with a power rating of 25 watts and equipped with a run-capacitor of 1.1 μF ;
- A voltage-source inverter employing an H-bridge configuration;
- A monitoring system for voltage and current based on an NI-6009 data-collecting device and a laptop;
- An STM32F4 discovery board.

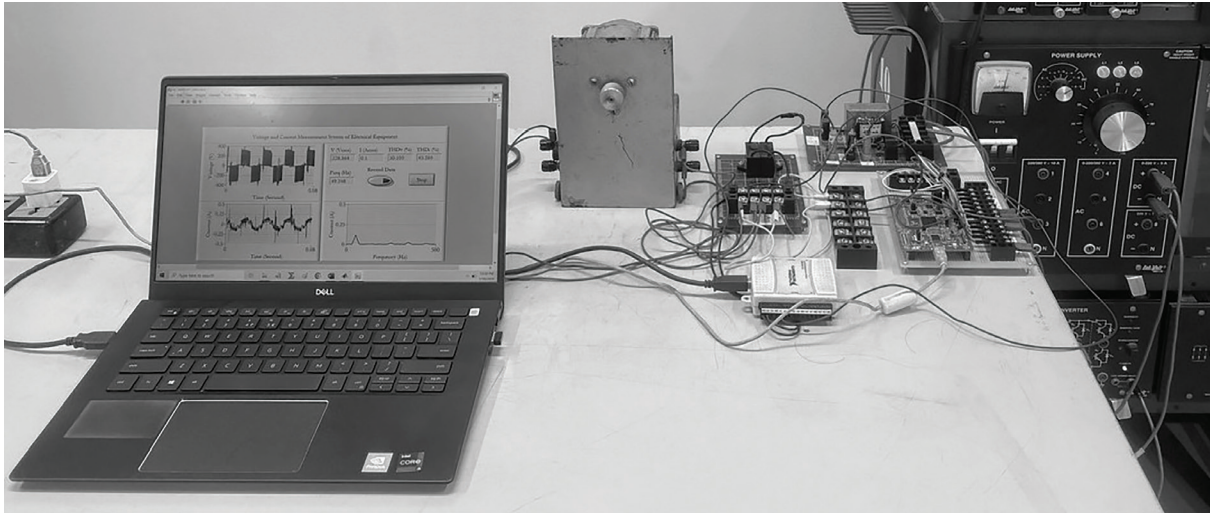


Figure 8. The experimental system.

4.1. Parameter estimation of the SPIM

A single-phase electronic meter manufactured by LS Company (Republic of Korea) was used to measure the parameters of single-phase loads, including the voltage, current and active power. To obtain the root-mean-square values of the voltage and current of the main and auxiliary windings, the following procedure was carried out:

- Connecting the single-phase electronic meter to measure the voltage, current and active power of the motor input under the no-load test and recording V_{NL}^{in} , I_{NL}^{in} and P_{NL}^{in} ,
- Connecting the single-phase electronic meter to measure the voltage, current and active power of the motor input under the locked rotor test and recording V_{LR}^{in} , I_{LR}^{in} and P_{LR}^{in} ,
- Connecting the single-phase electronic meter to measure the voltage, current and active power of the main winding under the no-load test and recording V_{NL}^m , I_{NL}^m and P_{NL}^m ,
- Connecting the single-phase electronic meter to measure the voltage, current and active power of the main winding under the locked rotor test and recording V_{LR}^m , I_{LR}^m and P_{LR}^m ,
- Connecting the single-phase electronic meter to measure the voltage, current and active power of the auxiliary winding under the no-load test and recording V_{NL}^a , I_{NL}^a and P_{NL}^a ,
- Connecting the single-phase electronic meter to measure the voltage, current and active power of the auxiliary winding under the locked rotor test and recording V_{LR}^a , I_{LR}^a and P_{LR}^a .

Tables 2 and 3 show recorded operational characteristics of the main and auxiliary windings, and the input to the stator during the no-load and locked rotor tests. The motor briefly operated under the locked rotor test. The motor input power under the locked rotor test is approximately 2.5 of it under the no-load test. These tables were utilised for estimating the parameters of the motor.

Tables 4 and 5 indicate calculated parameters of the main and auxiliary windings, respectively. Table 6 displays the first 20 iterations of the Nelder–Mead method used to minimise the objective function (21). Upon achieving convergence, the Nelder–Mead approach reveals the ideal values for the key winding parameters, which are presented in Tables 7 and 8.

The mechanical parameters can be determined by conducting a dynamic simulation of the motor. The moment of inertia of the rotor is closely correlated with the transient state of the motor. Meanwhile, the friction factor is associated with the motor's stable condition. Upon doing multiple experiments, the mechanical parameters possess the subsequent values:

- The moment of inertia of the rotor: $J = 2.5 \times 10^{-4} \text{ (kg/m}^2\text{)}$;
- The coefficient of friction: $F = 5.3 \times 10^{-4} \text{ (N/m/s)}$.

Table 2. Motor operation parameters measured under the no-load test.

	$V(V)$	$I(A)$	$P(W)$
Main winding	227	0.12	10.1
Auxiliary winding	227	0.13	10.4
Stator input	227	0.09	20.5

Table 3. Motor operation parameters measured under the locked rotor test.

	$V(V)$	$I(A)$	$P(W)$
Main winding	227	0.27	53
Auxiliary winding	227	0.12	2
Stator input	227	0.25	55.1

Table 4. Estimated parameters of the equivalent circuit of the main winding.

$R_s^m(\Omega)$	$X_{ls}^m(\Omega)$	$X_s^m(\Omega)$	$X_{lr}^m(\Omega)$	$R_r^m(\Omega)$
338	221.117	2,247	221.117	400.023

Table 5. Estimated parameters of the equivalent circuit of the auxiliary winding.

$R_s^a(\Omega)$	$X_{ls}^a(\Omega)$	$X_s^a(\Omega)$	$X_{lr}^a(\Omega)$	$R_r^a(\Omega)$
138	943.281	7,062.3	943.281	4.888

Table 6. The first 20 iterations of the Nelder–Mead method.

Iteration	Func-count	min f(x)	Procedure
0	1	109.248	
1	5	99.1460	Initial simplex
2	7	83.9113	Expand
3	9	57.8937	Expand
4	10	57.8937	Reflect
5	12	19.2787	Expand
6	14	16.7708	Reflect
7	16	8.07153	Reflect
8	17	8.07153	Reflect
9	19	8.07153	Contract inside
10	21	8.07153	Contract inside
11	23	6.93307	Contract inside
12	25	6.93307	Contract inside
13	27	6.02920	Reflect
14	29	6.02920	Contract inside
15	31	3.52893	Contract inside
16	32	3.52893	Reflect
17	34	3.52893	Contract outside
18	36	3.52893	Contract inside
19	38	1.90971	Contract inside
20	40	1.90971	Contract inside

Table 7. Improved estimated parameters of the equivalent circuit of the main winding using the Nelder–Mead method.

$R_s^m (\Omega)$	$X_{ls}^m (\Omega)$	$X_s^m (\Omega)$	$X_{lr}^m (\Omega)$	$R_r^m (\Omega)$
327	189.553	2,361.8	168.781	475.451

Table 8. Improved estimated parameters of the equivalent circuit of the auxiliary winding using the Nelder–Mead method.

$R_s^a (\Omega)$	$X_{ls}^a (\Omega)$	$X_s^a (\Omega)$	$X_{lr}^a (\Omega)$	$R_r^a (\Omega)$
134	1,067.3	4,296.7	1,012.3	4.9

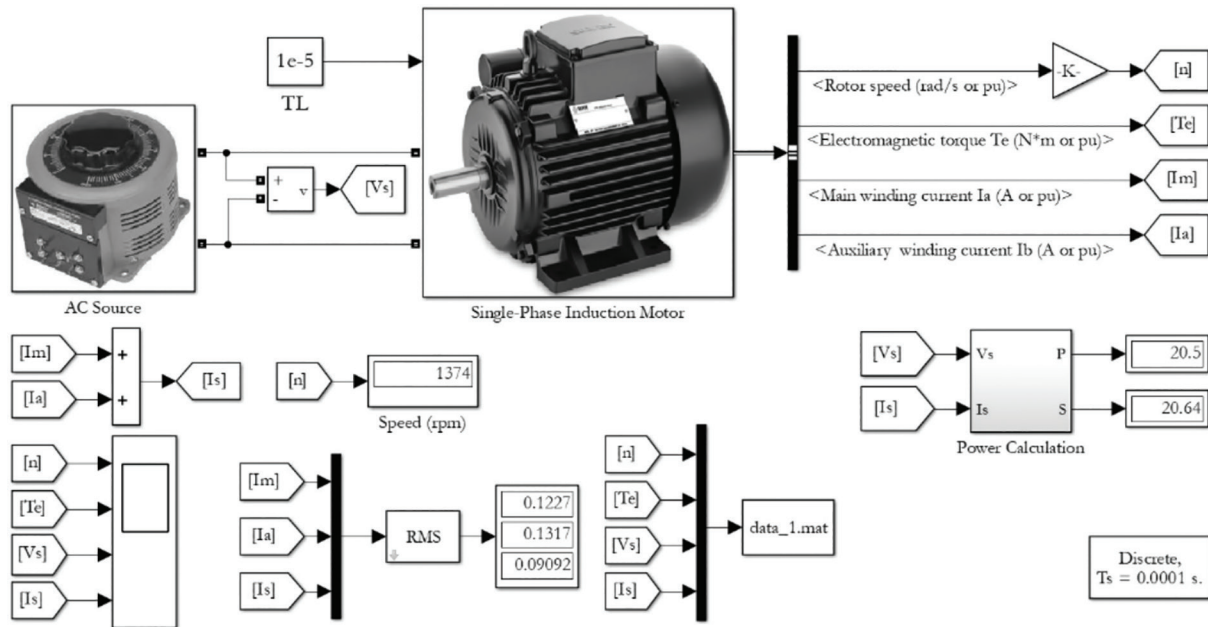


Figure 9. Dynamic simulation of the SPIM in Simulink. SPIM, single-phase induction motor.

Figure 9 depicts the Simulink diagram of the SPIM, which is used to verify the enhanced parameter estimation of the motor. Table 9 displays the motor parameters obtained from both simulated and measured data during the no-load test. Table 10 displays the motor parameters obtained from both simulation and measurement during the locked rotor test. These data include the current in the main winding $I_m (A)$, the current in the auxiliary winding $I_a (A)$, the input current of the motor $I_s (A)$ and the input actual power of the motor $P_s (W)$.

4.2. Scalar control of the SPIM

4.2.1. Simulation

The speed of the motor can be regulated by employing an H-bridge single-phase inverter using the scalar control technique. The speed of the motor depending on the frequency of the inverter output voltage has the following form:

$$n = (1 - s) \frac{60f}{p} \tag{35}$$

where n is the motor rotor speed, f is the frequency of the inverter output voltage, p is the number of motor pole pairs and s is the slip rate. When changing the frequency, there is also a need to vary the output inverter voltage to avoid the motor from the over current. Therefore, the frequency and value of the voltage at the inverter output

Table 9. Simulated and measured motor parameters under the no-load test.

	I_m (A)	I_a (A)	I_s (A)	P_s (W)
Simulated values	0.122	0.131	0.09	20.4
Measured values	0.12	0.13	0.09	20.5

Table 10. Simulated and measured motor parameters under the locked rotor test.

	I_m (A)	I_a (A)	I_s (A)	P_s (W)
Simulated values	0.271	0.118	0.246	55.73
Measured values	0.27	0.12	0.25	55.1

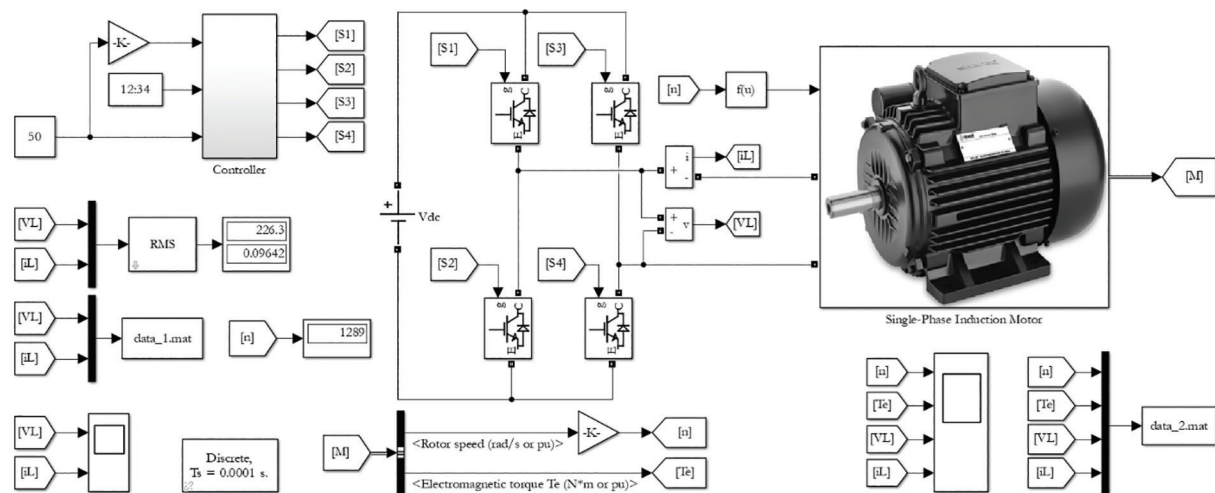


Figure 10. Dynamic simulation of the SPIM fed by a single-phase H-bridge inverter in Simulink. SPIM, single-phase induction motor.

must be changed simultaneously. One of the popular techniques to change the voltage and frequency is sinusoidal pulse width modulation (SPWM).

Figure 10 shows the Simulink diagram of an SPIM fed by a single-phase H-bridge inverter. The inverter regulates the output voltage by employing the SPWM. This technique involves utilising a triangle carrier wave with a frequency that is 27 times higher than the sine modulation wave. Figure 11 displays graphical representations of the motor voltage and current. The ratio of the amplitude of the modulation wave to that of the carrier wave is defined as the modulation index, which is given as follows:

$$m = \frac{A_m}{A_c} \tag{36}$$

where A_m is the amplitude of the modulation wave and A_c is the amplitude of the carrier wave. The reference signal of the SPWM has the following form:

$$V_{ref} = \frac{mf}{f_1} \sin(2\pi ft) \tag{37}$$

in which f_1 is the maximum frequency of the modulation wave and f is the frequency of the modulation wave to reduce the motor speed ($f \leq f_1$). If $f = f_1 = 50$ (Hz), then V_{ref} yields as follows:

$$V_{ref} = m \sin(2\pi 50t) \tag{38}$$

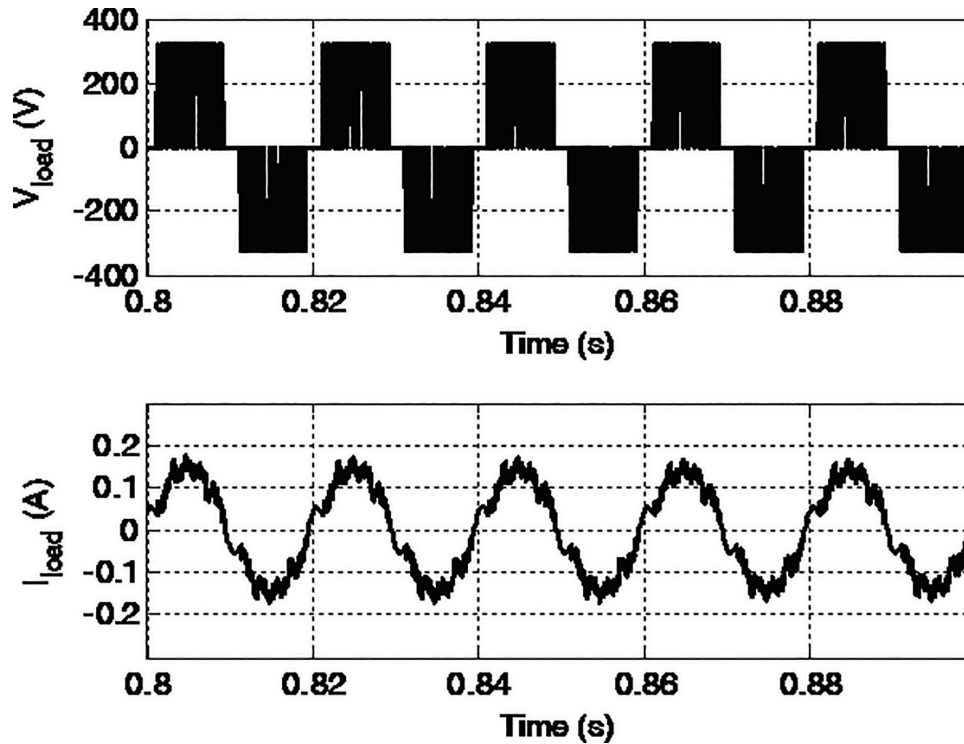


Figure 11. Simulated waveforms of the load voltage and current.

Table 11. The motor speed according to the change in the frequency of the modulation wave.

f (Hz)	m	V_s (V)	I_s (A)	n (rpm)
50	0.8	226.3	0.0967	1,298
45	0.8	220.5	0.0976	1,132
40	0.8	208.0	0.1048	979
35	0.8	188.0	0.1078	814
30	0.8	170.8	0.0967	661
25	0.8	164.7	0.0967	521
20	0.8	150.1	0.0959	282
15	0.8	130.0	0.0923	96

As the number of poles of the motor is 2, then the speed of the motor is slightly smaller than 1,500 (rpm). The value of m is chosen to be 0.8 to obtain the rated motor input current of 0.1 (A). Table 11 displays the change in motor speed according to different values of the frequency of the modulation wave. Figure 12 is the change in motor speed according to the variation in the frequency of the modulation wave.

4.2.2. Experiment

The scalar control algorithm of the SPIM in the experiment relies on the STM32F4 discovery board, which can be directly programmed using the MATLAB Simulink, as depicted in Figure 13. The library for programming the STM32F4 discovery board in the Simulink is available online (Waijung 1 [STM32 target]). The load voltage and current waveforms are depicted in Figure 14. Compared with the waveform of the simulated load current, the waveform of the actual load current has more noise. Table 12 compares the root-mean-square values of the simulated and actual waveforms for the load voltage and current. The simulated and actual values of the load voltage and load current are quite identical.

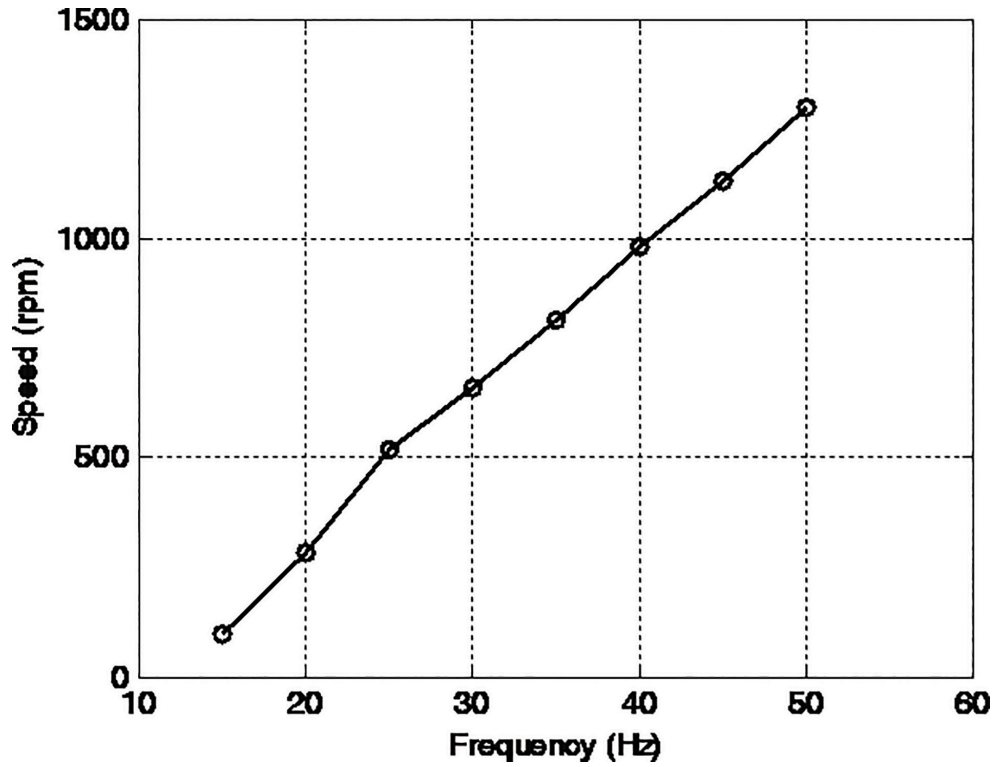


Figure 12. The motor speed versus frequency of the modulation wave.

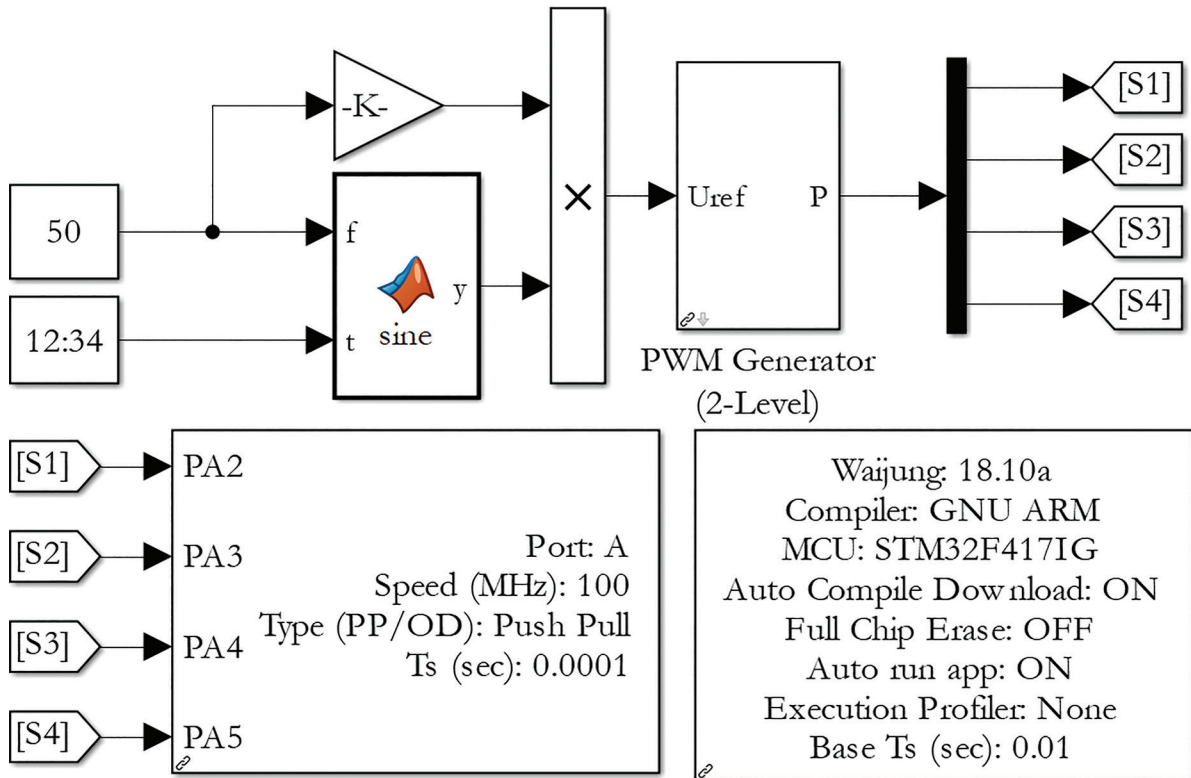


Figure 13. Simulink diagram for deploying the V/F constant control method on the STM32F4 discovery board.

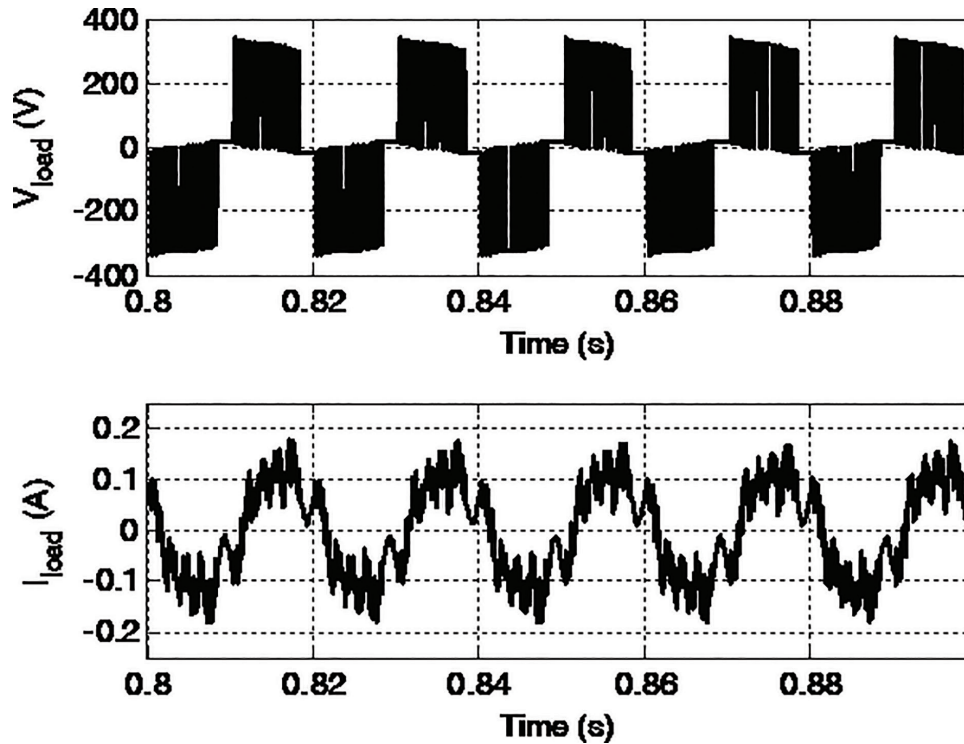


Figure 14. Actual waveforms of the load voltage and current.

Table 12. Comparison between the simulated and actual results of the load voltage and current.

	V_L (A)	I_L (A)
Simulated values	226	0.1031
Measured values	226	0.0915

5. Conclusions

This paper presents a well-defined methodology for accurately estimating the parameters of an SPIM in an offline setting. The proposed method can be implemented using a cost-effective experimental set-up utilising the Nelder–Mead method, which is a non-derivative optimisation technique. Measurement tests were conducted to acquire the initial condition for the Nelder–Mead optimisation algorithm. Next, the ultimate characteristics of the motor were determined by the process of minimising two objective functions that quantifies the disparity between the measured and predicted input impedance of the equivalent circuits of the main and auxiliary windings. Subsequent research for this study will focus on examining the impact of temperature increase in the stator and rotor windings on the calculation of motor parameters necessary for the high-performance vector control of SPIMs.

Acknowledgements

This research is funded by Hanoi University of Science and Technology (HUST) under Project No. T2023-PC-041.

References

- Aller, J. M., Viola, J. C., Restrepo, J. A., Fajardo, M., Ginart, A., Rengifo, J. W., Loja, J. D. and Ochoa, J. D. (2018). Space vector control of asymmetrical single-phase induction motors. In: *2018 XIII International Conference on Electrical Machines ICEM*, Alexandroupoli, Greece, 3-6 Sep 2018.
- Almani, M. N., Hussain, G. A. and Zaher, A. A. (2021). An Improved Technique for Energy-Efficient Starting and Operating Control of Single Phase Induction Motors. *IEEE Access*, 9, pp. 12446–12462. doi: 10.1109/ACCESS.2021.3050920
- Asadabadi, Y., Arab Markadeh, G. R., Soltani, J. and Heidari, R. (2011). Efficiency control of single phase induction motor drive. In: *International Aegean Conference on Electrical Machines and Power Electronics and Electromotion, Joint Conference*, Istanbul, Turkey, 8-10 Sep 2011.
- Bhowmick, D., Manna, M. and Chowdhury, S. (2018). Estimation of Equivalent Circuit Parameters of Transformer and Induction Motor from Load Data. *IEEE Transactions on Industry Applications*, 54(3), pp. 2784–2791. doi: 10.1109/TIA.2018.2790378
- Correa, M. B., Jacobina, C. B., da Silva, E. R. C. and Lima, A. M. N. (2004). Vector Control Strategies for Single-Phase Induction Motor Drive Systems. *IEEE Transactions on Industrial Electronics*, 51(5), pp. 1073–1080. doi: 10.1109/TIE.2004.834973
- Dangeam, S. and Kinnares, V. (2015). A direct torque control for three-leg voltage source inverter fed asymmetrical single-phase induction motor. In: *2015 18th International Conference on Electrical Machines and Systems ICEMS*, Pattaya, Thailand, 21 Jan 2016.
- Ghial, V. K., Saini, L. M. and Saini, J. S. (2014). Parameter Estimation of Permanent-Split Capacitor-Run Single-Phase Induction Motor Using Computed Complex Voltage Ratio. *IEEE Transactions on Industrial Electronics*, 61(2), pp. 682–692. doi: 10.1109/TIE.2013.2253067
- Huynh, P., Zhu, H. and Aliprantis, D. (2015). Non-intrusive parameter estimation for single-phase induction motors using transient data. In: *2015 IEEE Power and Energy Conference at Illinois PECE*, Champaign, IL, USA, 20-21 Feb 2015.
- Jang, D. (2013). Problems Incurred in a Vector-Controlled Single-Phase Induction Motor, and a Proposal for a Vector-Controlled Two-Phase Induction Motor as a Replacement. *IEEE Transactions on Power Electronics*, 28(1), pp. 526–536. doi: 10.1109/TPEL.2012.2199772
- Jannati, M. and Fallah, E. (2011). A new method for speed sensorless vector control of single-phase induction motor using Extended Kalman Filter. In: *2011 19th Iranian Conference on Electrical Engineering*, Tehran, Iran, 17-19 May 2011.
- Jemli, M., Azza, H. B., Boussak, M. and Gossa, M. (2009). Sensorless Indirect Stator Field Orientation Speed Control for Single-Phase Induction Motor Drive. *IEEE Transactions on Power Electronics*, 24(6), pp. 1618–1627. doi: 10.1109/TPEL.2009.2014867
- Jidin, A. Lazi, J. M., Abdullah, A. R., Patkar, F., Fazliana Abd Kadir, A. and Mat Hanafiah, M. A. (2005). Speed drive based on torque-slip characteristic of the single phase induction motor. In: *2005 International Conference on Power Electronics and Drives Systems*, Kuala Lumpur, Malaysia, 01 Dec 2005.
- Kim, K., Lim, S. B. and Lee, J. (2009). Design of rotor slot of single phase induction motor with copper die-cast rotor cage for high efficiency. In: *INTELEC 2009 – 31st International Telecommunications Energy Conference*, Incheon, Korea, 11 Dec 2009.
- Lagarias, J. C., Reeds, J. A., Wright, M. H. and Wright, P. E. (1998). Convergence Properties of the Nelder-Mead Simplex Method in Low Dimensions. *SIAM Journal of Optimization*, 9(1), pp. 112–147. doi: 10.1137/S1052623496303470
- Nied, A., de Oliveira, J., Stival, L. H. R. C. and Polli, H. B. (2013). Improving washing machine performance using single-phase induction motor field-oriented control. In: *IECON 2013 – 39th Annual Conference of the IEEE Industrial Electronics Society*, Vienna, Austria, 10-13 Nov 2013.
- Ojaghi, M. and Daliri, S. (2016). Analytic Model for Performance Study and Computer-Aided Design of Single-Phase Shaded-Pole Induction Motors. *IEEE Transactions on Energy Conversion*, 32(2), pp. 649–657. doi: 10.1109/TEC.2016.2645641
- Poudel, B., Shiwakoti, R., Amiri, E., Rastgoufard, P., Field, T. E. and Ramamurthy, J. (2019). Aggregate model of single phase induction motors. In: *2019 IEEE International Electric Machines & Drives Conference IEMDC*, San Diego, CA, USA, 12-15 May 2019.
- Rahman, S., Meraj, M., Iqbal, A., Tariq, M., Maswood, A. I., Ben-Brahim, L. and Al-ammari, R. (2020). Design and Implementation of Cascaded Multilevel qZSI Powered Single-Phase Induction Motor for Isolated Grid Water Pump Application. *IEEE Transactions on Industry Applications*, 56(2), pp. 1907–1917. doi: 10.1109/TIA.2019.2959734

- Rubio-Astorga, G., Sánchez-Torres, J. D., Cañedo, J. and Loukianov, A. G. (2014). High-Order Sliding Mode Block Control of Single-Phase Induction Motor. *IEEE Transactions on Control Systems Technology*, 22(5), pp. 1828–1836. doi: 10.1109/TCST.2013.2289307
- Saneie, H. and Nasiri-Gheidari, Z. (2021). Performance Analysis of Outer-Rotor Single-Phase Induction Motor Based on Magnetic Equivalent Circuit. *IEEE Transactions on Industrial Electronics*, 68(2), pp. 1046–1054. doi: 10.1109/TIE.2020.2969125
- Schraud, J., Fuchs, E. F. and Fuchs, H. A. (2008). Experimental Verification of Critical-Speed Increase of Single-Phase Induction Machines via Winding Reconfiguration with Solid-State Switches. *IEEE Transactions on Energy Conversion*, 23(2), pp. 460–465. doi: 10.1109/TEC.2008.921476
- Sharma, U. and Singh, B. (2021). Design and Development of Energy Efficient Single Phase Induction Motor for Ceiling Fan Using Taguchi's Orthogonal Arrays. *IEEE Transactions on Industry Applications*, 57(4), pp. 3562–3572. doi: 10.1109/TIA.2021.3072020
- Sutedjo, Qudsi, O. A., Rosalina, I. I., Yanaratri, D. S. and Suhariningsih. (2018). V/f SPWM inverter for single-phase induction motor controller using adaptive neuro-fuzzy inference system. In: *2018 3rd International Conference on Information Technology, Information System and Electrical Engineering ICITISEE*, Yogyakarta, Indonesia, 13-14 Nov 2018.
- Um, D. Y. and Park, G. S. (2019). Determination Scheme of Stator Parameters for Making Rotating Fields Circular in a Single-Phase Induction Motor. *IEEE Transactions on Magnetics*, 56(1).
- Vendrusculo, E. A. and Pomilio, J. A. (2008). An adaptive speed estimator for single-phase induction motors. In: *2008 International Symposium on Power Electronics, Electrical Drives, Automation and Motion*, Ischia, Italy, 11-13 Jun 2008.
- Vieira, R. P., Azzolin, R. Z. and Grundling, H. A. (2009). Parameter identification of a single-phase induction motor using RLS algorithm. In: *2009 Brazilian Power Electronics Conference*, Bonito-Mato Grosso do Sul, Brazil, 27 Sep 2009.
- Waijung 1. (STM32 target). Available at: <https://www.aimagin.com/en/download>
- Wang, X., Zhong, H., Yang, Y. and Mu, X. (2010). Study of a Novel Energy Efficient Single-Phase Induction Motor with Three Series-Connected Windings and Two Capacitors. *IEEE Transactions on Energy Conversion*, 25(2), pp. 433–440. doi: 10.1109/TEC.2009.2039218
- Zahedi, B. and Vaez-Zadeh, S. (2009). Efficiency Optimization Control of Single-Phase Induction Motor Drives. *IEEE Transactions on Power Electronics*, 24(4), pp. 1062–1070. doi: 10.1109/TPEL.2008.2011639